

Eigenmode Analysis of Boundary Conditions for the One-dimensional Preconditioned Euler Equations

David L. Darmofal
Massachusetts Institute of Technology

Pierre Moinier and Michael B. Giles
Oxford University Computing Laboratory

The effect of local preconditioning on boundary conditions is analyzed for the subsonic, one-dimensional Euler equations. Decay rates for the eigenmodes of the initial boundary value problem are determined for different boundary conditions and different preconditioners whose intent is to accelerate low Mach number computations. Riemann invariant boundary conditions based on the unpreconditioned Euler equations are shown to be reflective when used with preconditioning, and asymptotically, at low Mach numbers, initial disturbances do not decay. Other boundary conditions are shown to be perfectly non-reflective in conjunction with preconditioning. Two-dimensional numerical results confirm the trends predicted by the one-dimensional analysis.

Key words and phrases: boundary conditions, preconditioning, convergence acceleration, Euler equations

Oxford University Computing Laboratory
Numerical Analysis Group
Wolfson Building
Parks Road
Oxford, England OX1 3QD

March, 2000

1 Introduction

Local preconditioning has been successfully utilized to accelerate the convergence to a steady-state for Euler and Navier-Stokes simulations [1, 2, 3, 4, 5, 6, 7, 8, 9]. Local preconditioning is introduced into a time-dependent problem as,

$$\mathbf{u}_t + \mathbf{P} \mathbf{r}(\mathbf{u}) = 0,$$

‘ where \mathbf{u} is the state vector of length m , \mathbf{r} is the residual vector of length m , and \mathbf{P} is the $m \times m$ preconditioning matrix which may depend on \mathbf{u} in nonlinear problems. Since preconditioning effectively alters the time-dependent properties of the governing partial differential equation, modifications to the numerical discretization can be required. For example, upwind methods for inviscid problems must be based on the characteristics of the preconditioned equations instead of the unpreconditioned equations [2]. Similarly, the behavior of boundary conditions in conjunction with preconditioning will also be altered. While the affect of preconditioning on boundary conditions is known [10, 11, 12], to date, no quantitative analysis has been performed.

The purpose of this paper is to analyze the effect of preconditioning on several different boundary conditions commonly used in numerical simulations. Specifically, we consider the one-dimensional, preconditioned Euler equations linearized about a steady, uniform, subsonic mean state. The work is an extension of the analysis of Giles [13] for the one-dimensional, unpreconditioned Euler equations by which the exact eigenmodes and eigenfrequencies of the initial boundary value problem can be analytically determined. From these, we find the exponential decay rates for initial perturbations under different sets of boundary conditions. In addition to reviewing Giles’ analysis for the Euler equations, we analyze the Euler equations preconditioned by the Van Leer/Lee/Roe[2] and Turkel[1] preconditioners. Turkel has proposed and analyzed a number of different low Mach number preconditioners; the one considered here is that developed by Weiss and Smith [4] and subsequently used by many others[6, 7, 9]. Finally, we demonstrate the validity of the analysis through numerical results for a two-dimensional application.

2 Theory

We start with a review of the analysis of the initial boundary value problem by Giles [13]. The linearized Euler equations are given by,

$$\begin{pmatrix} \tilde{\rho} \\ \tilde{q} \\ \tilde{p} \end{pmatrix}_T + \begin{pmatrix} \bar{q} & \bar{\rho} & 0 \\ 0 & \bar{q} & \bar{\rho}^{-1} \\ 0 & \bar{\rho} \bar{c}^2 & \bar{q} \end{pmatrix} \begin{pmatrix} \tilde{\rho} \\ \tilde{q} \\ \tilde{p} \end{pmatrix}_X = 0, \quad (2.1)$$

where $\tilde{\rho}$, \tilde{q} , \tilde{p} are the perturbations to the density, velocity, and pressure, and $\bar{\rho}$, \bar{q} , \bar{c} are the undisturbed density, velocity, and speed of sound, which is related to the pressure and density through $\bar{c}^2 = \gamma \bar{p} / \bar{\rho}$. The subsonic inflow is located at $X = 0$ and the outflow is at $X = L$.

Next, we define the following non-dimensionalizations to simplify the analysis,

$$\rho \equiv \frac{\tilde{\rho}}{\bar{\rho}}, \quad q \equiv \frac{\tilde{q}}{\bar{c}}, \quad p \equiv \frac{\tilde{p}}{\bar{\rho}\bar{c}^2}, \quad x \equiv \frac{X}{L}, \quad t \equiv \frac{T}{L/\bar{c}}. \quad (2.2)$$

The non-dimensional version of Equation (2.1) is

$$\mathbf{u}_t + \mathbf{A}\mathbf{u}_x = 0, \quad (2.3)$$

where,

$$\mathbf{u} = \begin{pmatrix} \rho \\ q \\ p \end{pmatrix}, \quad \mathbf{A} = \begin{pmatrix} M & 1 & 0 \\ 0 & M & 1 \\ 0 & 1 & M \end{pmatrix},$$

and M is the undisturbed Mach number \bar{q}/\bar{c} .

The boundary conditions for subsonic flow require two inflow quantities and one outflow quantity to be specified. The inflow boundary conditions can be expressed as,

$$\mathbf{C}_{in}\mathbf{u}(0, t) = 0, \quad (2.4)$$

where \mathbf{C}_{in} is a 2×3 matrix dependent on the specific choice of inflow conditions. Similarly, the single outflow boundary condition can be expressed as,

$$\mathbf{C}_{out}\mathbf{u}(1, t) = 0, \quad (2.5)$$

where \mathbf{C}_{out} is a 1×3 matrix dependent on the specific choice of outflow condition.

Equations (2.3), (2.4) and (2.5) represent the initial boundary value problem for the unpreconditioned Euler equations. An eigenmode of the initial boundary value problem is given by,

$$\mathbf{u} = e^{-i\omega t} \sum_{j=1}^3 \alpha_j e^{i\omega x/\lambda_j} \mathbf{r}_j. \quad (2.6)$$

\mathbf{r}_j and λ_j are the right eigenvectors and eigenvalues, respectively, of the matrix \mathbf{A} , i.e.,

$$(\mathbf{A} - \lambda_j \mathbf{I}) \mathbf{r}_j = 0.$$

In the following developments, we assume that the eigenvalues have been ordered such that the two forward-moving characteristics are $j=1, 2$ (i.e. $\lambda_{1,2} > 0$) and the backward-moving characteristic is $j=3$ (i.e. $\lambda_3 < 0$). The eigenfrequency ω and characteristic strengths α_j are determined by the boundary conditions. For the inflow boundary, substitution of Equation (2.6) into Equation (2.4) leads to,

$$\begin{pmatrix} b_{11} & b_{12} & b_{13} \\ b_{21} & b_{22} & b_{23} \end{pmatrix} \begin{pmatrix} \alpha_1 \\ \alpha_2 \\ \alpha_3 \end{pmatrix} = 0, \quad (2.7)$$

where

$$\begin{pmatrix} b_{11} & b_{12} & b_{13} \\ b_{21} & b_{22} & b_{23} \end{pmatrix} = \mathbf{C}_{in} \begin{pmatrix} \mathbf{r}_1 & \mathbf{r}_2 & \mathbf{r}_3 \end{pmatrix}. \quad (2.8)$$

A necessary condition for the well-posedness of the initial boundary value problem is that the incoming characteristics, α_1 and α_2 , can be determined as functions of the outgoing characteristic, α_3 . This requires that the 2×2 matrix,

$$\begin{pmatrix} b_{11} & b_{12} \\ b_{21} & b_{22} \end{pmatrix}$$

is non-singular. Also, the boundary condition at the inflow will be non-reflecting if the outgoing characteristic does not cause a perturbation in the incoming characteristics. Thus the condition to be non-reflecting is that $b_{13} = b_{23} = 0$.

For the outflow boundary, substitution of Equation (2.6) into Equation (2.5) leads to,

$$\begin{pmatrix} b_{31} & b_{32} & b_{33} \end{pmatrix} \begin{pmatrix} \alpha_1 \\ \alpha_2 \\ \alpha_3 \end{pmatrix} = 0, \quad (2.9)$$

where

$$\begin{pmatrix} b_{31} & b_{32} & b_{33} \end{pmatrix} = \mathbf{C}_{out} \begin{pmatrix} e^{i\omega/\lambda_1} \mathbf{r}_1 & e^{i\omega/\lambda_2} \mathbf{r}_2 & e^{i\omega/\lambda_3} \mathbf{r}_3 \end{pmatrix}. \quad (2.10)$$

In this case, well-posedness of the initial boundary value problem requires that the incoming characteristic, α_3 , can be determined as a function of the outgoing characteristics, α_1 and α_2 . Thus, b_{33} must be non-zero. Also, the boundary condition at the outflow will be non-reflecting if $b_{31} = b_{32} = 0$.

The inflow and outflow boundary conditions in Equations (2.7) and (2.9) can be combined as,

$$\mathbf{B}(\omega) \begin{pmatrix} \alpha_1 \\ \alpha_2 \\ \alpha_3 \end{pmatrix} = 0. \quad (2.11)$$

In order for a non-trivial solution of the initial boundary value problem to exist, a non-zero vector, $(\alpha_1, \alpha_2, \alpha_3)^T$, must exist which satisfies Equation (2.11). This is possible only for values of ω for which,

$$\det \mathbf{B}(\omega) = 0.$$

Separating the eigenfrequency into its real and imaginary parts, $\omega = \omega_r + i\omega_i$, the amplitude of the eigenmodes grows as $\exp(\omega_i t)$. Thus, for the eigenmodes to decay, we require that $\omega_i < 0$ for all eigenfrequencies. We also note that the steady-state problem is well-posed if, and only if, $\det \mathbf{B}(0)$ is non-zero [13].

Within a computational simulation, one indicator of the convergence rate is actually the decay per time step or cycle. Assuming the time step is given by a CFL condition of the form $\Delta t = \nu \Delta x / \lambda_{\max}$ where ν is a constant dependent on the temporal integration, Δx is the cell size, and λ_{\max} is the maximum amplitude eigenvalue, then $\omega_i \Delta t = \omega_i / \lambda_{\max} \nu \Delta x$. Since ν and Δx depend on the iterative scheme and the computational grid, respectively, we will use $\omega_i / \lambda_{\max}$ as a measure of convergence rate since this ratio only depends on the governing flow equations and the corresponding boundary conditions. In the following, we will refer to $\omega_i / \lambda_{\max}$ as the rate of decay or decay rate. Note, a more traditional measure of convergence rate is the decay factor per cycle. If

the decay factor per cycle were solely due to the propagation of solution error out of the computational domain, then the decay factor would be,

$$\begin{aligned}\text{decay factor} &= \exp(\omega_i \Delta t), \\ &= \exp\left(\frac{\omega_i}{\lambda_{\max}} \nu \Delta x\right).\end{aligned}$$

The above is the analysis for the unpreconditioned Euler equations. When using preconditioning the non-dimensional p.d.e. becomes

$$\mathbf{u}_t + \mathbf{P}\mathbf{A}\mathbf{u}_x = 0, \quad (2.12)$$

and so the right eigenvectors and associated eigenvalues are defined by

$$(\mathbf{P}\mathbf{A} - \lambda_j \mathbf{I}) \mathbf{r}_j = 0.$$

The rest of the analysis remains unaltered.

3 Analysis

3.1 No preconditioning

In the absence of any preconditioning the eigenvalues of \mathbf{A} are $\lambda_{1,2,3} = M, M+1, M-1$, and the eigenvectors are

$$\begin{pmatrix} \mathbf{r}_1 & \mathbf{r}_2 & \mathbf{r}_3 \end{pmatrix} = \begin{pmatrix} 1 & 1 & 1 \\ 0 & 1 & -1 \\ 0 & 1 & 1 \end{pmatrix}. \quad (3.1)$$

The first eigenmode corresponds to the convection of an entropy variation. The other two modes correspond to acoustic waves traveling downstream and upstream, respectively. The maximum eigenvalue is $\lambda_{\max} = M+1$ corresponding to the downstream-running acoustic wave.

3.1.1 Riemann boundary conditions

We first consider the specification of Riemann invariants at both boundaries. In their original nonlinear dimensional form, these are

$$\begin{aligned}X = 0, \quad & \begin{cases} p'/\rho'^\gamma = \bar{p}/\bar{\rho}^\gamma, \\ q' + \frac{2}{\gamma-1}c' = \bar{q} + \frac{2}{\gamma-1}\bar{c}, \end{cases} \\ X = L, \quad & q' - \frac{2}{\gamma-1}c' = \bar{q} - \frac{2}{\gamma-1}\bar{c},\end{aligned}$$

where the primed quantities are the sum of the undisturbed state and the corresponding perturbation, e.g. $p' = \bar{p} + \tilde{p}$. Linearization and non-dimensionalization of the boundary conditions gives,

$$\mathbf{C}_{in} = \begin{pmatrix} -1 & 0 & 1 \\ -1 & \gamma-1 & \gamma \end{pmatrix}, \quad \mathbf{C}_{out} = \begin{pmatrix} 1 & \gamma-1 & -\gamma \end{pmatrix}.$$

from which we obtain the matrix \mathbf{B} ,

$$\mathbf{B} = \begin{pmatrix} -1 & 0 & 0 \\ -1 & 2(\gamma-1) & 0 \\ e^{i\omega/\lambda_1} & 0 & -2(\gamma-1)e^{i\omega/\lambda_3} \end{pmatrix}.$$

b_{13} and b_{23} are both equal to zero, so the inflow boundary condition is perfectly non-reflecting. On the other hand, b_{31} is non-zero so the outflow boundary condition is partially reflecting. Consequently, all initial perturbations will disappear entirely in the finite time it takes for the entropy characteristic to convect from the inflow to the outflow, plus the time it takes for the reflected upstream-propagating acoustic wave to reach the inflow.

This complete decay of initial perturbations in a finite time is mirrored in the fact that the determinant of \mathbf{B} is

$$\det \mathbf{B} = 4(\gamma-1)^2 e^{i\omega/\lambda_3},$$

and setting this equal to zero would require that $\omega_i = -\infty$, giving an infinite rate of exponential decay.

3.1.2 Entropy, stagnation enthalpy at inflow; pressure at outflow

Another common set of boundary conditions for subsonic, internal flows is the specification of entropy and stagnation enthalpy at the inflow and pressure at the outflow. For these boundary conditions, we obtain

$$\mathbf{C}_{in} = \begin{pmatrix} -1 & 0 & 1 \\ -1 & (\gamma-1)M & \gamma \end{pmatrix}, \quad \mathbf{C}_{out} = \begin{pmatrix} 0 & 0 & 1 \end{pmatrix},$$

and hence

$$\mathbf{B} = \begin{pmatrix} -1 & 0 & 0 \\ -1 & (\gamma-1)(1+M) & (\gamma-1)(1-M) \\ 0 & e^{i\omega/\lambda_2} & e^{i\omega/\lambda_3} \end{pmatrix}.$$

The eigenfrequencies are determined by

$$\det \mathbf{B} = (\gamma-1) [(1-M)e^{i\omega/\lambda_2} - (1+M)e^{i\omega/\lambda_3}] = 0.$$

which gives

$$\omega = \frac{1-M^2}{2} \left[-i \log \left(\frac{1+M}{1-M} \right) + 2n\pi \right], \quad \text{for integer } n.$$

Thus there is an infinite set of discrete eigenfrequencies, all with the negative growth rate

$$\omega_i = -\frac{1-M^2}{2} \log\left(\frac{1+M}{1-M}\right) \Rightarrow \omega_i/\lambda_{\max} = -\frac{1-M}{2} \log\left(\frac{1+M}{1-M}\right),$$

proving that all initial disturbances will decay exponentially to zero. Note however that as $M \rightarrow 0$ the rate of decay also tends towards zero, implying that the convergence rate for numerical computations will become poor at low Mach numbers.

3.1.3 Velocity, temperature at inflow; pressure at outflow

The final set of boundary conditions we consider is setting the velocity and temperature at the inflow and the pressure at the outflow. For these boundary conditions, which are fairly common in low speed viscous flow applications, we get

$$\mathbf{C}_{in} = \begin{pmatrix} 0 & 1 & 0 \\ -1 & 0 & \gamma \end{pmatrix}, \quad \mathbf{C}_{out} = \begin{pmatrix} 0 & 0 & 1 \end{pmatrix},$$

and

$$\mathbf{B} = \begin{pmatrix} 0 & 1 & -1 \\ -1 & 0 & (\gamma-1)M \\ 0 & e^{i\omega/\lambda_2} & e^{i\omega/\lambda_3} \end{pmatrix}.$$

Equating the determinant to zero gives

$$\omega = (1-M^2) \left(n + \frac{1}{2}\right) \pi, \quad \text{for integer } n.$$

The purely real nature of ω means that initial disturbances do not decay as time proceeds. In practice, initial disturbances in a numerical computation would probably die out due to the action of numerical smoothing, but the convergence would be exceedingly slow, and would get very much worse as the grid is refined.

3.2 Van Leer/Lee/Roe preconditioner

With the one-dimensional version of the Van Leer/Lee/Roe preconditioner [2, 14], the resultant \mathbf{PA} matrix is,

$$\mathbf{PA} = \begin{pmatrix} M & 0 & -2M \\ 0 & M & 2 \\ 0 & 0 & -M \end{pmatrix}.$$

The specific form of \mathbf{P} is described in the Appendix. The eigenvalues of \mathbf{PA} are $\lambda_{1,2,3} = M, M, -M$, and the eigenvectors are,

$$\begin{pmatrix} \mathbf{r}_1 & \mathbf{r}_2 & \mathbf{r}_3 \end{pmatrix} = \begin{pmatrix} 1 & 0 & M \\ 0 & 1 & -1 \\ 0 & 0 & M \end{pmatrix}. \quad (3.2)$$

3.2.1 Riemann boundary conditions

The boundary condition matrices \mathbf{C}_{in} and \mathbf{C}_{out} are unaffected by the preconditioning, but the change to the eigenvectors means that \mathbf{B} is now

$$\mathbf{B} = \begin{pmatrix} -1 & 0 & 0 \\ -1 & \gamma-1 & (\gamma-1)(M-1) \\ e^{i\omega/M} & (\gamma-1)e^{i\omega/M} & -(\gamma-1)(M+1)e^{-i\omega/M} \end{pmatrix}.$$

In contrast to the unpreconditioned Euler equations, b_{23} and b_{32} are now both non-zero, and so the Riemann boundary conditions are reflective for the preconditioned Euler equations. The determinant of \mathbf{B} is,

$$\det \mathbf{B} = -(\gamma-1)^2 [(M-1)e^{i\omega/M} + (M+1)e^{-i\omega/M}],$$

and the eigenfrequencies which result in a zero determinant are

$$\begin{aligned} \omega_r &= Mn\pi, & \text{for integer } n, \\ \omega_i &= -\frac{M}{2} \log \left(\frac{1+M}{1-M} \right). \end{aligned}$$

Since $\lambda_{\max} = M$ for this preconditioned system,

$$\omega_i/\lambda_{\max} = -\frac{1}{2} \log \left(\frac{1+M}{1-M} \right).$$

In particular, we note that as $M \rightarrow 0$, $\omega_i/\lambda_{\max} \rightarrow 0$. Thus, at low Mach numbers, disturbances will not decay rapidly, indicating that the use of Riemann boundary conditions based on the Euler equations is likely to impede convergence to a steady state.

3.2.2 Entropy, stagnation enthalpy at inflow; pressure at outflow

For these boundary conditions, we obtain

$$\mathbf{B} = \begin{pmatrix} -1 & 0 & 0 \\ -1 & (\gamma-1)M & 0 \\ 0 & 0 & Me^{-i\omega/M} \end{pmatrix}.$$

We note that $b_{13} = b_{23} = b_{31} = b_{32} = 0$. Thus, outgoing waves do not generate any reflections at either the inflow or outflow boundaries. Disturbances are eliminated in the time it takes for all of the characteristics to propagate from one end to the other. This is verified by setting the determinant of \mathbf{B} equal to zero,

$$\det \mathbf{B} = -(\gamma-1)M^2 e^{-i\omega/M} = 0,$$

which requires that $\omega_i = -\infty$. This is in contrast to the results for the unpreconditioned Euler equations for which the boundary conditions are reflective, and the exponential decay rate is finite.

This surprising result can be further understood by considering the preconditioned equations re-written with entropy (s), stagnation enthalpy (H), and pressure (p) as the dependent states. These equations (with appropriate non-dimensionalization) are

$$\begin{pmatrix} s \\ H \\ p \end{pmatrix}_t + \begin{pmatrix} M & 0 & 0 \\ 0 & M & 0 \\ 0 & 0 & -M \end{pmatrix} \begin{pmatrix} s \\ H \\ p \end{pmatrix}_x = 0. \quad (3.3)$$

Thus, the preconditioned Euler equations are a set of decoupled advection equations for entropy, stagnation enthalpy, and pressure in which entropy and stagnation enthalpy propagate downstream and the pressure propagates upstream. Hence, these boundary conditions are actually characteristic boundary conditions and non-reflective.

3.2.3 Velocity, temperature at inflow; pressure at outflow

For these boundary conditions, we find that

$$\mathbf{B} = \begin{pmatrix} 0 & 1 & -1 \\ -1 & 0 & (\gamma-1)M \\ 0 & 0 & Me^{-i\omega/M} \end{pmatrix}.$$

Comparing this to the matrix \mathbf{B} without preconditioning, the significant difference is that b_{32} is zero, in addition to b_{31} , and so the outflow boundary condition is now perfectly non-reflecting (i.e. $\omega_i = -\infty$). This is because the upstream propagating characteristic wave is a pressure perturbation (see Equation (3.3)), and so the imposition of the exit pressure fixes the value of the upstream propagating characteristic.

The non-reflecting outflow boundary condition results as usual in the elimination of initial transients within a finite time, in marked contrast to the unpreconditioned behavior in which the initial transients persist indefinitely. The fact that the inflow boundary condition is reflecting means that the finite convergence time is equal to the sum of the times taken for characteristics to travel up and down the domain, which is precisely double that required when specifying the entropy and stagnation enthalpy instead at the inflow boundary.

3.3 Turkel preconditioner

For the one-dimensional form of the Turkel preconditioner[1] employed by Weiss and Smith [4], the resultant \mathbf{PA} matrix is,

$$\mathbf{PA} = \begin{pmatrix} M & \epsilon & M(\epsilon-1) \\ 0 & M & 1 \\ 0 & \epsilon & M\epsilon \end{pmatrix}.$$

The specific form of \mathbf{P} is again described in the Appendix. The eigenvalues of \mathbf{PA} are

$$\lambda_1 = M, \quad \lambda_2 = \frac{1}{2}(M(1+\epsilon) + \tau), \quad \lambda_3 = \frac{1}{2}(M(1+\epsilon) - \tau),$$

with $\tau = \sqrt{(1-\epsilon)^2 M^2 + 4\epsilon}$, and the eigenvectors are

$$\begin{pmatrix} \mathbf{r}_1 & \mathbf{r}_2 & \mathbf{r}_3 \end{pmatrix} = \begin{pmatrix} 1 & 1 & 1 \\ 0 & \frac{M(1-\epsilon)+\tau}{2\epsilon} & \frac{M(1-\epsilon)-\tau}{2\epsilon} \\ 0 & 1 & 1 \end{pmatrix}.$$

To make the three eigenvalues of the same order of magnitude at low Mach numbers, it is usual to define ϵ to be

$$\epsilon = \min\{1, \eta M^2\}. \quad (3.4)$$

where η is a constant typically taken from $1 \leq \eta \leq 4$. Note that when $\epsilon=1$, \mathbf{P} reduces to the identity matrix. Therefore, the definition of ϵ ensures that the preconditioning is switched off in a continuous manner when the Mach number reaches $1/\sqrt{\eta}$.

3.3.1 Riemann boundary conditions

The matrix \mathbf{B} is

$$\mathbf{B} = \begin{pmatrix} -1 & 0 & 0 \\ -1 & (\gamma-1) \left[\frac{M(1-\epsilon)+\tau}{2\epsilon} + 1 \right] & (\gamma-1) \left[\frac{M(1-\epsilon)-\tau}{2\epsilon} + 1 \right] \\ e^{i\omega/\lambda_1} & (\gamma-1) \left[\frac{M(1-\epsilon)+\tau}{2\epsilon} - 1 \right] e^{i\omega/\lambda_2} & (\gamma-1) \left[\frac{M(1-\epsilon)-\tau}{2\epsilon} - 1 \right] e^{i\omega/\lambda_3} \end{pmatrix},$$

and hence the eigenfrequencies which make its determinant equal to zero are

$$\begin{aligned} \omega_r &= \frac{\lambda_2 \lambda_3}{\lambda_3 - \lambda_2} 2n\pi, \quad \text{for integer } n, \\ \omega_i &= -\frac{\lambda_2 \lambda_3}{\lambda_3 - \lambda_2} \log \left(\frac{\epsilon + 1 + \tau}{\epsilon + 1 - \tau} \right). \end{aligned}$$

Thus, since the largest eigenvalue is $\lambda_{\max} = \lambda_2$,

$$\omega_i / \lambda_{\max} = -\frac{\lambda_3}{\lambda_3 - \lambda_2} \log \left(\frac{\epsilon + 1 + \tau}{\epsilon + 1 - \tau} \right).$$

Since $\lambda_2 \lambda_3 / (\lambda_3 - \lambda_2)$ is positive, this means there is a finite rate of exponential decay of initial transients, due to the reflective nature of the boundary conditions in conjunction with the Turkel preconditioner. Even worse, as $M \rightarrow 0$, $\frac{\epsilon+1+\tau}{\epsilon+1-\tau} \rightarrow 1$ and so the rate of decay tends to zero at low Mach numbers indicating very poor convergence to the steady state. Note that,

$$\frac{\lambda_3}{\lambda_3 - \lambda_2} = \frac{1}{2} \left[1 - \frac{M}{\tau} (1 + \epsilon) \right],$$

and as $M \rightarrow 0$, $\lambda_3 / (\lambda_3 - \lambda_2) \rightarrow \frac{1}{2}(1 - 1/\sqrt{1+4\eta})$ which remains finite.

3.3.2 Entropy, stagnation enthalpy at inflow; pressure at outflow

The matrix \mathbf{B} is

$$\mathbf{B} = \begin{pmatrix} -1 & 0 & 0 \\ -1 & (\gamma-1) \left[\frac{M^2(1-\epsilon)+M\tau}{2\epsilon} + 1 \right] & (\gamma-1) \left[\frac{M^2(1-\epsilon)-M\tau}{2\epsilon} + 1 \right] \\ 0 & e^{i\omega/\lambda_2} & e^{i\omega/\lambda_3} \end{pmatrix},$$

and hence the eigenfrequencies are

$$\begin{aligned} \omega_r &= \frac{\lambda_2 \lambda_3}{\lambda_3 - \lambda_2} 2n\pi, \quad \text{for integer } n, \\ \omega_i &= -\frac{\lambda_2 \lambda_3}{\lambda_3 - \lambda_2} \log \left[\frac{M^2(1-\epsilon) + 2\epsilon + M\tau}{M^2(1-\epsilon) + 2\epsilon - M\tau} \right], \\ \omega_i/\lambda_{\max} &= -\frac{\lambda_3}{\lambda_3 - \lambda_2} \log \left[\frac{M^2(1-\epsilon) + 2\epsilon + M\tau}{M^2(1-\epsilon) + 2\epsilon - M\tau} \right]. \end{aligned}$$

These boundary conditions give a finite rate of exponential decay when used with the Turkel preconditioner. In addition, as $M \rightarrow 0$, $\frac{M^2(1-\epsilon)+2\epsilon+M\tau}{M^2(1-\epsilon)+2\epsilon-M\tau} \rightarrow \frac{1+2\eta+\sqrt{1+4\eta}}{1+2\eta-\sqrt{1+4\eta}}$ and so the rate of decay remains finite. However, this is still not quite as good as the finite time convergence achieved with the same boundary conditions in conjunction with the Van Leer/Lee/Roe preconditioner.

3.3.3 Velocity, temperature at inflow; pressure at outflow

The matrix \mathbf{B} is

$$\mathbf{B} = \begin{pmatrix} -1 & \gamma-1 & \gamma-1 \\ 0 & \frac{M(1-\epsilon)+\tau}{2\epsilon} & \frac{M(1-\epsilon)-\tau}{2\epsilon} \\ 0 & e^{i\omega/\lambda_2} & e^{i\omega/\lambda_3} \end{pmatrix},$$

and so the eigenfrequencies are

$$\begin{aligned} \omega_r &= \frac{\lambda_2 \lambda_3}{\lambda_3 - \lambda_2} (2n+1)\pi, \quad \text{for integer } n, \\ \omega_i &= -\frac{\lambda_2 \lambda_3}{\lambda_3 - \lambda_2} \log \left[\frac{\tau + M(1-\epsilon)}{\tau - M(1-\epsilon)} \right], \\ \omega_i/\lambda_{\max} &= -\frac{\lambda_3}{\lambda_3 - \lambda_2} \log \left[\frac{\tau + M(1-\epsilon)}{\tau - M(1-\epsilon)} \right]. \end{aligned}$$

When $M \rightarrow 0$, $\frac{\tau+M(1-\epsilon)}{\tau-M(1-\epsilon)} \rightarrow \frac{\sqrt{1+4\eta}+1}{\sqrt{1+4\eta}-1}$ and so the rate of decay remains finite and any initial disturbance will decay exponentially.

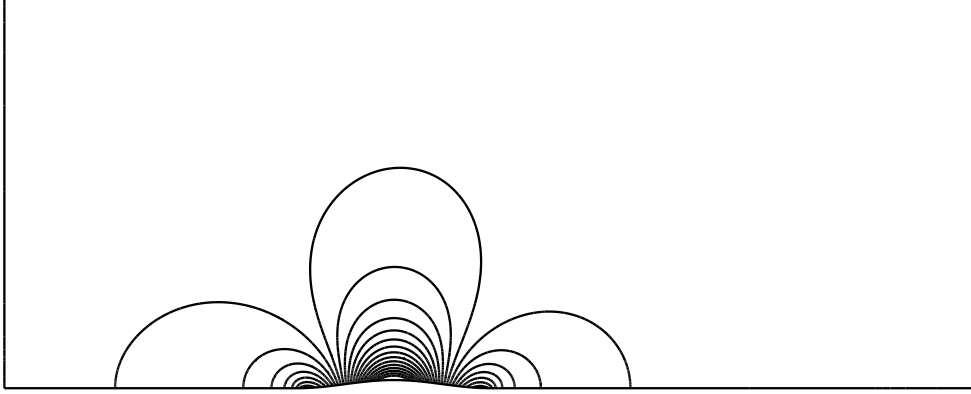
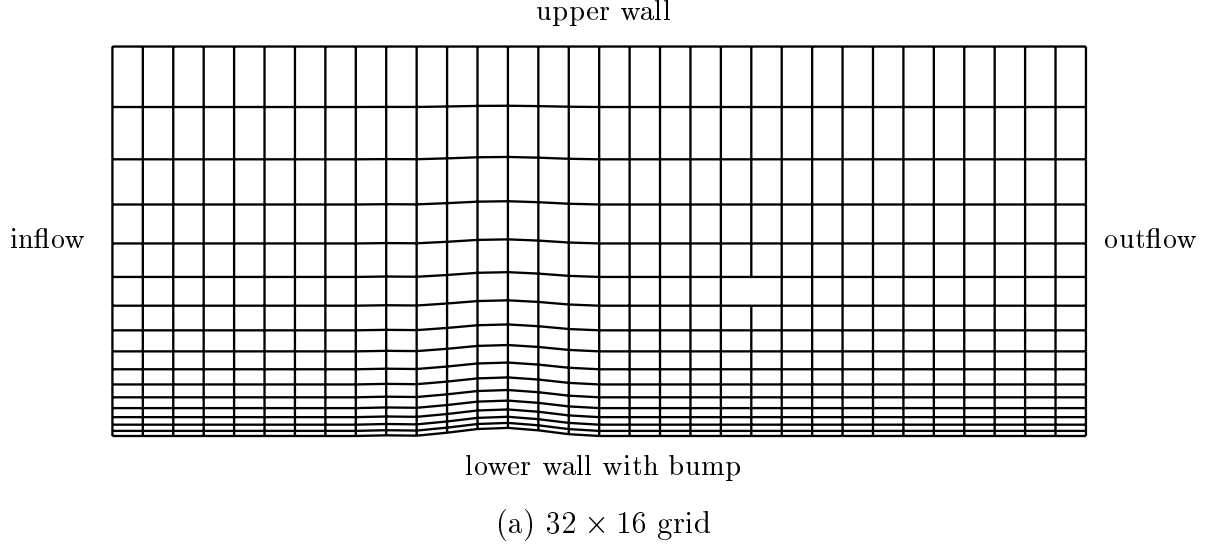


Figure 1: Sample duct grid and pressure coefficient data.

4 Numerical Results

To illustrate the effect of different boundary conditions on numerical convergence as well as check the accuracy of the analysis, we simulate the two-dimensional flow in a duct with a straight upper wall and a bump on the lower wall between $0 \leq x \leq 1$ described by $y = 0.042 \sin^2(\pi x)$. The domain is 5 unit lengths long and 2 lengths high. The grid is structured with clustering toward the wall boundary.

We use the numerical algorithm described by Darmofal and Siu [9] which employs the semi-coarsening technique of Mulder [15, 16] in conjunction with a multi-stage, block Jacobi relaxation [17, 18]. The discretization is a 2nd order upwind scheme with a Roe approximate Riemann solver [19]. The calculations are performed on a grid of 32×16 cells. A three level, V-cycle is utilized with 2 pre- and post-smoothing iterations at each level. All calculations are initialized to uniform flow. The grid and a typical distribution

of pressure coefficient are shown in Figure 1.

The Turkel preconditioner analyzed in Section 3.3 is used in the simulations. As opposed to the ϵ definition given in Equation (3.4), Darmofal and Siu[9] have found slightly better convergence is obtained for a block Jacobi iterative scheme when ϵ is given by,

$$\epsilon_{cut} = \begin{cases} M^2/(1 - \alpha_{cut}^2 M^2) & \text{for } M < M_{cut}, \\ 1 & \text{for } M \geq M_{cut}, \end{cases} \quad (4.1)$$

where $\alpha_{cut}^2 = (1 - M_{cut}^2)/M_{cut}^2$ and M_{cut} is the user-defined Mach number above which no preconditioning is used. For the results in this paper, we use $M_{cut} = 0.5$. For this definition of ϵ , the value of ω_i/λ_{\max} is plotted versus Mach number in Figure 2 (a) for the three sets of boundary conditions. For the Euler Riemann boundary conditions, the decay rate clearly approaches zero as $M \rightarrow 0$; however, as $M \rightarrow 0.5$, preconditioning is turned off and the Riemann boundary conditions are non-reflective (thus, $\omega_i/\lambda_{\max} \rightarrow -\infty$). The entropy, enthalpy, and pressure boundary conditions (SHP) have a finite rate of decay and for $M < 0.3$ have the fastest decay rate of the three sets of boundary conditions. Above this Mach number, the Riemann boundary conditions are the fastest decaying. Finally, the velocity, temperature, and pressure (QTP) boundary conditions have a finite rate of decay for low Mach numbers but as $M \rightarrow 0.5$, $\omega_i \rightarrow 0$. For $M > 0.2$, the QTP boundary conditions have the slowest rate of decay of the three boundary conditions.

We have implemented the boundary conditions described above by constructing a boundary face state vector and calculating the boundary flux directly from this state vector. For example, at an inflow for the SHP boundary conditions, entropy, enthalpy, and the tangential velocity are prescribed from the exterior and the pressure is extrapolated from the interior. At an outflow, we reverse the procedure and specify pressure from the exterior and extrapolate entropy, enthalpy, and tangential velocity from the interior. Note, regardless of the specific boundary conditions, we always use the tangential velocity as the additional variable for the two-dimensional boundary implementation.

The number of cycles required to converge the solution six orders of magnitude from the initial residual are given in Table 1. Also, the convergence behavior is plotted in Figure 2(b). Specifically, we plot the variation of $-1/\text{cycles}$ which would be proportional to the analytic decay rate in Figure 2(a) if the analysis was a reasonable model of the computation. As can be clearly seen, the analytical and computational results behave quite similarly. At low Mach numbers, the Riemann boundary conditions are unstable while the SHP boundary conditions perform best. The velocity, temperature, pressure boundary (QTP) conditions are about 75% more expensive than the SHP conditions for low Mach numbers. At the higher Mach numbers, the Riemann boundary condition cases begin to converge and the number of cycles decreases with increasing Mach number. In particular, the Riemann boundary conditions converge faster than the QTP and SHP boundary conditions for approximately $M > 0.3$ and 0.45 , respectively.

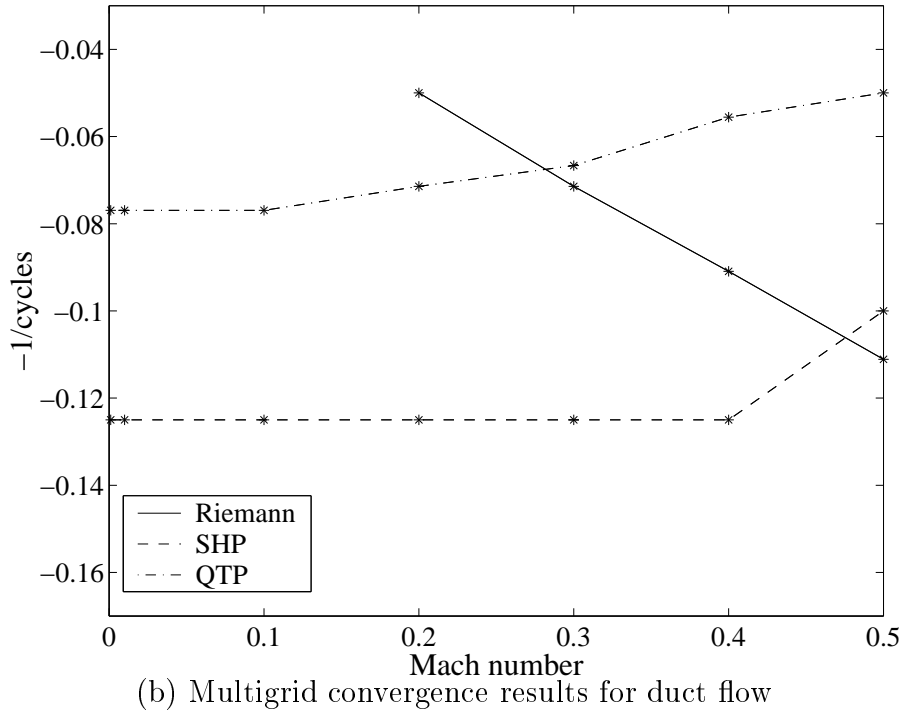
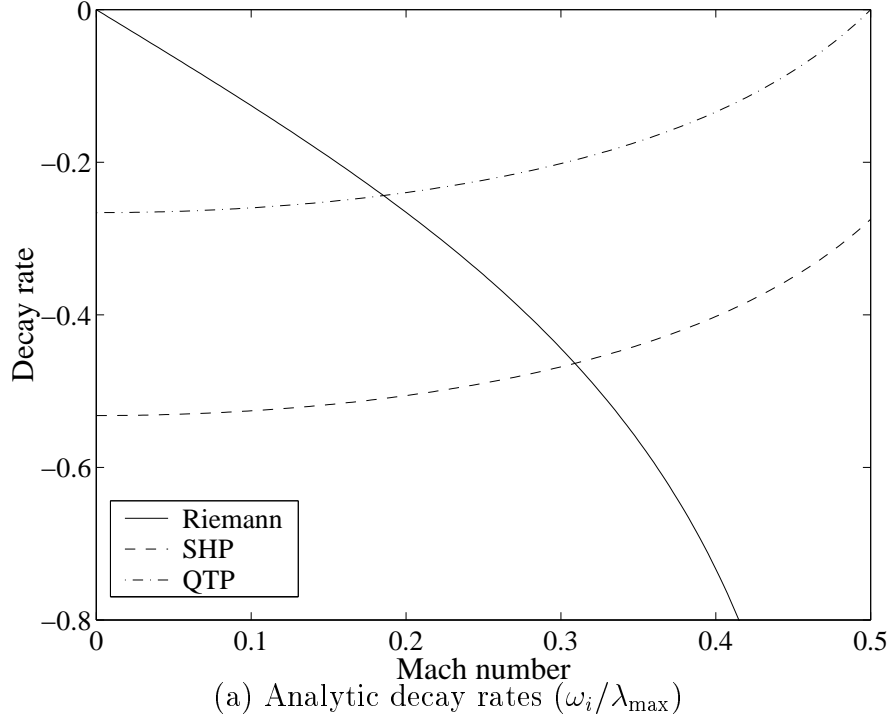


Figure 2: Boundary condition effect on analytic decay rates and multigrid convergence for Turkel preconditioner. Riemann: Euler Riemann invariant boundary conditions (Section 3.1.1). SHP: entropy, enthalpy, pressure boundary conditions (Section 3.1.2). QTP: velocity, temperature, pressure boundary conditions (Section 3.1.3).

Mach	Riemann	SHP	QTP
0.001	UNS	8	13
0.01	UNS	8	13
0.1	UNS	8	13
0.2	20	8	14
0.3	14	8	15
0.4	11	8	18
0.5	9	10	20

Table 1: Number of cycles required to drop residual six orders of magnitude for different Mach numbers and boundary conditions. Riemann: Euler Riemann invariant boundary conditions from Section 3.1.1. SHP: entropy, enthalpy, pressure boundary conditions from Section 3.1.2. QTP: velocity, temperature, pressure boundary conditions from Section 3.1.3. UNS: algorithm was unstable and aborted with infinite residual.

5 Final remarks

The present analysis of the Euler equations with two forms of low Mach number preconditioning shows the quite significant effect of the preconditioning on the effectiveness of boundary conditions in eliminating initial transients.

Boundary conditions based on the Riemann invariants of the Euler equations are found to be reflective in conjunction with preconditioning, whereas they are non-reflecting at the inflow without it; the problem is most detrimental at low Mach numbers where the perturbation decay rate approaches zero.

Boundary conditions which specify entropy and stagnation enthalpy at an inflow and pressure at an outflow are found to be non-reflective with the Van Leer/Lee/Roe preconditioning, and weakly non-reflective in the other two cases. Numerical results confirm that this is the best of the three boundary conditions considered over a wide range of Mach numbers.

The specification of velocity and density at the inflow and pressure at the outflow is found to be non-reflecting for the Van Leer/Lee/Roe preconditioning and weakly reflective for the Turkel preconditioning. However, for the unpreconditioned Euler equations they provide no damping of initial transients in the absence of numerical smoothing.

There are many other boundary conditions which could have been considered. One possibility, which is particularly appropriate for airfoil applications in which the entire far-field flow state is known, would be to use linear characteristic boundary conditions. By design these are perfectly non-reflecting, but their construction is based upon the characteristic eigenvectors; changing the preconditioning therefore requires a change to the formulation of the boundary conditions. Pursuing this approach, in multiple dimensions the 1D characteristic boundary conditions will only be perfectly non-reflecting when the outgoing waves have wavecrests which are aligned with the boundary. To minimize the reflection when the wave incidence is not normal it would be possible to employ higher order methods which have been successfully developed for the Euler equations

[20, 21, 22].

Finally, for cases in which the particular choice of boundary conditions is determined by other factors, an interesting possibility would be to incorporate boundary condition considerations into the design of the preconditioner, so that the combination of the preconditioner and the boundary conditions is non-reflective.

References

- [1] E. Turkel. Preconditioned methods for solving the incompressible and low speed compressible equations. *Journal of Computational Physics*, 72:277–298, 1987.
- [2] B. Van Leer, W.T. Lee, and P.L. Roe. Characteristic time-stepping or local preconditioning of the Euler equations. AIAA Paper 91-1552, 1991.
- [3] Y.H. Choi and C.L. Merkle. The application of preconditioning in viscous flows. *Journal of Computational Physics*, 105:203–223, 1993.
- [4] J.M. Weiss and W.A. Smith. Preconditioning applied to variable and constant density flows. *AIAA Journal*, 33(11):2050–2057, 1995.
- [5] E. Turkel, V.N. Vatsa, and R. Radespiel. Preconditioning methods for low-speed flows. AIAA Paper 96-2460, 1996.
- [6] D. Jespersen, T. Pulliam, and P. Buning. Recent enhancements to OVERFLOW. AIAA Paper 97-0644, 1997.
- [7] D. Mavriplis. Multigrid strategies for viscous flow solvers on anisotropic unstructured meshes. AIAA Paper 97-1952, 1997.
- [8] D.L. Darmofal and B. Van Leer. Local preconditioning: Manipulating Mother Nature to fool Father Time. In M. Hafez and D.A. Caughey, editors, *Computing the Future II: Advances and Prospects in Computational Aerodynamics*. John Wiley and Sons, 1998.
- [9] D.L. Darmofal and K. Siu. A robust multigrid algorithm for the Euler equations with local preconditioning and semi-coarsening. *Journal of Computational Physics*, 151:728–756, 1999.
- [10] W.T. Lee. *Local preconditioning of the Euler equations*. PhD thesis, University of Michigan, 1991.
- [11] A.C. Godfrey. Steps toward a robust preconditioning. AIAA Paper 94-0520, 1994.
- [12] E. Turkel, R. Radespiel, and N. Kroll. Assessment of two preconditioning methods for aerodynamic problems. *Computers and Fluids*, 26:613–634, 1997.

- [13] M.B. Giles. Eigenmode analysis of unsteady one-dimensional Euler equations. ICASE Report No. 83-47, 1983.
- [14] D. Lee. *Local preconditioning of the Euler and Navier-Stokes equations*. PhD thesis, University of Michigan, 1996.
- [15] W.A. Mulder. A new approach to convection problems. *Journal of Computational Physics*, 83:303–323, 1989.
- [16] W.A. Mulder. A high resolution Euler solver based on multigrid, semi-coarsening, and defect correction. *Journal of Computational Physics*, 100:91–104, 1992.
- [17] J.F. Lynn and B. Van Leer. Multi-stage schemes for the Euler and Navier-Stokes equations with optimal smoothing. AIAA Paper 93-3355, 1993.
- [18] S.R. Allmaras. Analysis of a local matrix preconditioner for the 2-D Navier-Stokes equations. AIAA Paper 93-3330, 1993.
- [19] P.L. Roe. Approximate Riemann solvers, parametric vectors, and difference schemes. *Journal of Computational Physics*, 43:357–372, 1981.
- [20] B. Engquist and A. Majda. Absorbing boundary conditions for the numerical simulation of waves. *Mathematics of Computation*, 31:629–651, 1977.
- [21] M.B. Giles. Non-reflecting boundary conditions for Euler equation calculations. *AIAA Journal*, 28(12):2050–2058, 1990.
- [22] M.B. Giles. Non-reflecting boundary conditions for unsteady airfoil calculations. In *Proceedings of Third International Conference on Hyperbolic Problems*. Chartwell-Bratt, 1990.

Appendix

The one-dimensional Van Leer/Lee/Roe and Turkel preconditioners [14, 1] are usually derived using the symmetrizing variables which in dimensional form are $(\tilde{p}/\bar{\rho}\bar{c}, \tilde{q}, \tilde{p} - \bar{c}^2\tilde{\rho})$. Using Equation (2.2), the non-dimensional symmetrizing variables are,

$$\mathbf{v} = \begin{pmatrix} p & q & p - \rho \end{pmatrix}^T,$$

and are related to the $\mathbf{u} = (\rho, q, p)^T$ variables through the transformation, $\mathbf{v} = \mathbf{S}\mathbf{u}$, where,

$$\mathbf{S} = \begin{pmatrix} 0 & 0 & 1 \\ 0 & 1 & 0 \\ -1 & 0 & 1 \end{pmatrix}.$$

The preconditioned Euler equations in terms of \mathbf{v} are,

$$\mathbf{v}_t + \mathbf{P}_v \mathbf{A}_v \mathbf{v}_x = 0,$$

where, $\mathbf{P}_v = \mathbf{S}\mathbf{P}\mathbf{S}^{-1}$, and,

$$\mathbf{A}_v = \mathbf{S}\mathbf{A}\mathbf{S}^{-1} = \begin{pmatrix} M & 1 & 0 \\ 1 & M & 0 \\ 0 & 0 & M \end{pmatrix}.$$

The one-dimensional Van Leer/Lee/Roe preconditioner is given by,

$$\mathbf{P}_v = \begin{pmatrix} \frac{M^2}{\beta^2} & -\frac{M}{\beta^2} & 0 \\ -\frac{M}{\beta^2} & 1 + \frac{1}{\beta^2} & 0 \\ 0 & 0 & 1 \end{pmatrix},$$

which results in

$$\mathbf{P} = \mathbf{S}^{-1}\mathbf{P}_v\mathbf{S} = \begin{pmatrix} 1 & -\frac{M}{\beta^2} & \frac{M^2}{\beta^2} - 1 \\ 0 & 1 + \frac{1}{\beta^2} & -\frac{M}{\beta^2} \\ 0 & -\frac{M}{\beta^2} & \frac{M^2}{\beta^2} \end{pmatrix},$$

where $\beta^2 = 1 - M^2$.

The one-dimensional form of the Turkel preconditioner[1] employed by Weiss and Smith [4] is given by,

$$\mathbf{P}_v = \begin{pmatrix} \epsilon & 0 & 0 \\ 0 & 1 & 0 \\ 0 & 0 & 1 \end{pmatrix},$$

which results in

$$\mathbf{P} = \mathbf{S}^{-1}\mathbf{P}_v\mathbf{S} = \begin{pmatrix} 1 & 0 & \epsilon - 1 \\ 0 & 1 & 0 \\ 0 & 0 & \epsilon \end{pmatrix}.$$